Energy reflection by back-scattering and sputtering: total yields and angular distribution

J. Phys. D: Appl. Phys., 13 (1980) 1169–80. Printed in Great Britain

Energy reflection by back-scattering and sputtering: total yields and angular distribution

M M Jakas and M M R Williams†
Centro Atómico Bariloche, Instituto Balseiro, Universidad Nacional de Cuyo, 8400 SC de Bariloche, RN, Argentina

Received 29 October 1979

Abstract. The energy reflection coefficient—total yields and angular distributions—have been calculated by solving the transport equation for the average kinetic energy flux. The energy flux transported by projectiles and by recoils were evaluated separately, thus the back-scattering and sputtering contributions to the reflected energy were obtained. We have considered an infinite medium of stopping material and neglected the electronic energy loss as well as crystalline effects. The introduction of a power scattering law leads to the reduction of the integral equation for the energy flux to an algebraic system of equations for the spatial moments. An analytical treatment to evaluate the energy flux carried by the projectiles is also included. Good agreement was found between our theory and experiment, in particular with recently reported angular distributions of the reflected energy.

A special aspect of this work lies in the use of a synthetic kernel to represent the anisotropy of scattering in the laboratory system of co-ordinates.

1. Introduction

When ions with energy in the keV region strike a solid, a fraction of their energy can be re-emitted from the surface as kinetic energy of back-scattered particles and of sputtered atoms. This process can be described by the energy reflection coefficient R_E, which is the ratio of the re-emitted energy to that of the incoming ion. Accordingly, we may write:

$$R_E = R_{Eb} + R_{Es} \tag{1}$$

where R_{Eb} and R_{Es} are the fraction of the energy transported via back-scattering and sputtering, respectively. The contribution of the secondary electrons to the re-emitted energy can be omitted, since it can be suppressed experimentally, and also that carried by photons, which is negligible (Andersen 1970).

Direct measurements of R_E (Anderson 1970, Andersen *et al* 1976, Hildebrandt and Manns 1976, 1977, Schou *et al* 1978, Sorensen 1976, Sidenius 1974, Tanaka *et al* 1978) and theoretical evaluations (Sigmund 1968, Sigmund *et al* 1971, Littmark and Maderlechner 1976, Vukanic and Sigmund 1976, Williams 1979) are found in the literature for the materials that we will consider, i.e., amorphous and polycrystalline solids.

Theoretically, R_E has been obtained from the deposited energy distribution in an infinite medium. It was considered that the solid lies in the half-space $x>0$ and so the energy deposited in the $x<0$ region has been assumed to correspond to the reflected

† Permanent address: Nuclear Engineering Department, Queen Mary College, University of London.

0022-3727/80/071169+12 $01.50

energy. This procedure does not provide the values of the two components in equation (1) separately. In another approach R_{Eb} was evaluated using the single collision approximation (McCracken and Freeman 1969, Vukanic and Sigmund 1976), which is valid for light ions at large energies. At low energies, in the multiple collision range, the backscattering component was recently calculated making some simplifying assumption on the scattering law in order to keep evaluations analytical (Williams 1979). On the other hand, to our knowledge, no attempt has been made to calculate R_{Es}.

A novel situation arises from the experimental results (Hildebrandt and Manns 1977) for the angular distribution of the reflected energy. To deal theoretically with this problem the deposited energy is of no use, and the other procedures which are able, in principle, to give angular distributions, have not as yet been used to calculate the sputtering.

The purpose of this paper is to calculate each of the components of the reflected energy as well as their angular distributions. We will solve the transport equation for the average kinetic energy flux transported by projectiles and recoil atoms by assuming a power potential scattering law and neglecting electronic energy loss. A stopping material of infinite extent will be considered, and the integral transport equation will be reduced to an algebraic system of equations for the spatial moments using standard procedures (Winterbon *et al* 1970). Some analytical treatment will also be included. Details of the calculations are given in §2; §3 follows the discussion of our results and comparison of them with existing theories and experimental data.

2. Reduction of the transport equation

2.1. Basic equations

We consider an infinite and homogeneous medium with a unit source of particles with energy E and directional cosine μ, at $x=0$. Let us define the functions $F(x, \mu, E, \mu_0)$ and $F'(x, \mu, E, \mu_0)$ which are the kinetic energy flux transported by projectiles and recoil atoms moving within a directional cosine interval μ_0, $d\mu_0$ at x, respectively. These functions obey the backward transport equation:

$$\delta(x)\delta(\mu-\mu_0)E-\mu(\partial F/\partial x)=N\int d\sigma\,[F(x,\mu,E,\mu_0)-F(x,\mu',E-T,\mu_0)] \tag{2}$$

$$-\mu(\partial F'/\partial x)=N\int d\sigma[F'(x,\mu,E,\mu_0)-F'(x,\mu',E-T,\mu_0)-F''(x,\mu'',T,\mu_0)] \tag{3a}$$

where $F''(x, \mu, E, \mu_0)$ is the kinetic energy flux when projectile and target are of the same species. F'' obeys the equation:

$$\delta(x)\delta(\mu-\mu_0)E-\mu(\partial F''/\partial x) = N\int d\sigma[F''(x,\mu,E,\mu_0)-F''(x,\mu',E-T,\mu_0)-F''(x,\mu'',T,\mu_0)]. \tag{3b}$$

F'' appears because F' needs a source term, since originally there are no recoil particles moving.

The variables involved in equations (1)–(3) are the following: $d\sigma$ is the differential scattering cross-section; T is the energy lost by the scattered particle; μ' and μ'' are the directional cosines of the scattered particle and target atom respectively, after the collision; N is the atomic density of the stopping material.

2.2. Energy reflection coefficient

First of all, we can calculate the energy reflection coefficient from equations (1) and (2) multiplying them by $|\mu_0|$ and integrating over such a variable from -1 to 0. Hence, we obtain:

$$|\mu|\delta(x)\theta(-\mu)E-\mu(\partial G/\partial x)=N\int \mathrm{d}\sigma[G(x,E,\mu)-G(x,E-T,\mu')] \tag{4}$$

$$-\mu(\partial G'/\partial x)=N\int \mathrm{d}\sigma\,[G'(x,E,\mu)-G'(x,E-T,\mu')-G''(x,T,\mu'')] \tag{5a}$$

$$|\mu|\,\delta(x)\,\theta(-\mu)E-\mu(\partial G''/\partial x)=N\int \mathrm{d}\sigma[G''(x,E,\mu)-G''(x,E-T,\mu')-G''(x,T,\mu'')] \tag{5b}$$

where

$$G(x,E,\mu)=\int_{-1}^{0}\mathrm{d}\mu_0|\mu_0|\,F(x,E,\mu,\mu_0)$$

and the same for G' and G''. $\theta(x)$ is Heaviside's unit step function.

The functions G and G' evaluated at $x=0$ give us a measure of the energy reflected under ion bombardment due to back-scattered particles and sputtered atoms, respectively. Thus the energy reflection coefficient would be defined as follows:

$$R_{\mathrm{Eb}}=G(x=0,E,\mu)/E \tag{6}$$

$$R_{\mathrm{Es}}=G'(x=0,E,\mu)/E.$$

To solve equations (4–5) we follow the standard procedure (Winterbon *et al* 1970) introducing the power law scattering

$$N\sigma(E,T)=NC_mE^{-m}T^{-m-1}\qquad(0\leqslant m\leqslant 1)$$

and neglecting the electronic energy loss, we get the following algebraic systems of equations for the spatial moments expanded in Legendre polynomials in the cosine of the incidence angle:

$$S_l\delta_{n,0}+n\Delta_l g^{n-1}=(2l+1)g_l{}^n a_l{}^n \tag{7}$$

$$(2l+1)b_l{}^n g_l{}''^n(C_m/C'_m)^{n+1}+n\Delta_l g'^{n-1}=(2l+1)(a_l{}^n)g_l{}'^n \tag{8a}$$

$$S_l\delta_{n,0}+n\Delta_l g''^{n-1}=(2l+1)(a_l{}^n+b_l{}^n)g_l{}'^n. \tag{8b}$$

where $\Delta_l g^{n-1}$ means: $lg_{l-1}{}^{n-1}+(l+1)g_{l+1}{}^{n-1}$

$$g_l{}^n=G_l{}^n[E(E^{2m}/NC_m)^{n+1}]^{-1} \tag{9}$$

and

$$G_l{}^n=\tfrac{1}{2}\int_{-1}^{1}\mathrm{d}\mu\int_{-\infty}^{+\infty}x^n\,\mathrm{d}x G(x,E,\mu)\mathrm{P}_l(\mu)$$

where $\mathrm{P}_l(x)$ is the lth Legendre polynomial and similarly for $g_l{}'^n$ and g''^n.
For $g_l{}''$ it is necessary to replace C_m with $C_m{}'$ in equation (9), where $C_m{}'$ is the coefficient of the power law scattering when the ion is the same as the target. Furthermore, S_l is the projection of the source into the lth Legendre polynomial, and the coefficients $a_l{}^n$ and $b_l{}^n$ are defined as follows:

$$a_l{}^n=\int_0^{\gamma}\mathrm{d}x[1-(1-x)^{1+2m(n+1)}\mathrm{P}_l(g)]x^{-m-1}$$

$$b_l{}^n=\int_0^{\gamma}\mathrm{d}x(1-x)^{1+2m(n+1)}\mathrm{P}_l(g')x^{-m-1}.$$

$\gamma=4M_1M_2/(M_1+M_2)^2$, where M_1 and M_2 are the projectile and target mass, respectively.

The functions G and G' are reconstructed from their spatial moments by the polynomial approximation (Winterbon *et al* 1970)

$$G(x, E, \mu) \sim \sum_{l=0}^{N} \mathrm{H}_n(x') \exp(-x'^2) C_n \tag{10}$$

where $\mathrm{H}_n(x)$ are the Hermite polynomials of order n, and

$$x' = (x - \bar{x})/\sigma.$$

The parameters $\bar{x}$ and σ are those which minimise the expression

$$C_0^{-2} \sum_{n=0}^{N} C_n^2 n. \tag{11}$$

2.3. Angular distribution of the reflected energy

To deal with the angular distribution of the kinetic energy flux we could follow the same procedure; however, it can be applied only for the sputtering component, since the Legendre expansion for the back-scattered flux will converge poorly or not at all. To overcome this, we introduce the synthetic kernel approximation (SKA) (Williams 1978). We start from equation (2) and write explicitly the variables involved in the differential scattering cross-section, thus obtaining

$$\begin{aligned}\delta(x)\delta(\mu-\mu_0)E - \mu(\partial F/\partial x) \\ = N \int \sigma(E, T)\, \mathrm{d}T \delta[\bar{\Omega}.\bar{\Omega}' - g)][F(x, E, \mu, \mu_0) - F(x, E-T, \mu', \mu_0) \\ - F(x, T, \mu'', \mu_0)]\, \mathrm{d}\Omega'\end{aligned} \tag{12}$$

where $\bar{\Omega}$ and $\bar{\Omega}'$ are the directional vectors of the particle before and after the collision, respectively, and where g is the cosine of the scattering angle in the laboratory system. Introducing the synthetic kernel of order N which consists of the approximation

$$\delta(\bar{\Omega}.\bar{\Omega}' - g) \sim \sum_{l=0}^{N} [(2l+1)/2]\, \mathrm{P}_l(\bar{\Omega}.\bar{\Omega}')[\mathrm{P}_l(g) - \mathrm{P}_{N+1}(g)] + \mathrm{P}_{N+1}(g)\delta(\bar{\Omega}.\bar{\Omega}' - 1). \tag{13}$$

Equation (12) changes to

$$\begin{aligned}\delta(\mu-\mu_0)\delta(x)E - \mu(\partial F/\partial x) \\ = N \int \sigma(E, T)\, \mathrm{d}T[F(x, E, \mu, \mu_0) - F(x, \mu, E-T, \mu_0)\, \mathrm{P}_{N+1}(g)] \\ - \sum_{l=0}^{N} N(2l+1)\, \mathrm{P}_l(\mu) \int \sigma(E, T)\, T[\mathrm{P}_l(g) - \mathrm{P}_{N+1}(g)] F_l(x, E-T, \mu_0)\end{aligned} \tag{14}$$

where

$$F_l(x, E, \mu_0) = \tfrac{1}{2} \int_{-1}^{1} \mathrm{d}\mu\, \mathrm{P}_l(\mu) F(x, E, \mu, \mu_0).$$

Let us decompose F in two terms

$$F(x, E, \mu, \mu_0) = F^{\mathrm{I}}(\mu, E, x, \mu_0) + \delta(\mu - \mu_0) F^{\mathrm{s}}(E, x, \mu_0).$$

We insert them in equation (14) and after some algebra get

$$E\delta(x)-\mu_0(\partial F^{\mathrm{s}}/\partial x)$$
$$=N\int\sigma(E,T)\,\mathrm{d}T[F^{\mathrm{s}}(E,\mu_0,x)-F^{\mathrm{s}}(E-T,\mu_0,x)\,\mathrm{P}_{N+1}(g)] \tag{15}$$

$$-\mu\,(\partial F^{\mathrm{I}}/\partial x)=N\int\sigma(E,T)\,\mathrm{d}T[F^{\mathrm{I}}(x,\mu,E,\mu_0)-F^{\mathrm{I}}(x,E-T,\mu',\mu_0)\,\mathrm{P}_{N+1}(g)]$$
$$-\sum_{l=0}^{N}(2l+1)\,\mathrm{P}_l(\mu)N\int\sigma(E,T)\,\mathrm{d}T[\mathrm{P}_l(g)-\mathrm{P}_{N+1}(g)]F_l^{\mathrm{I}}(E-T,x,\mu_0)$$
$$-\tfrac{1}{2}\sum_{l=0}^{N}(2l+1)\mathrm{P}_l(\mu)\mathrm{P}_l(\mu_0)N\int\sigma(E,T)\,\mathrm{d}T[\mathrm{P}_l(g)-P_{N+1}(g)]F^{\mathrm{s}}(x,E-T,\mu_0). \tag{16}$$

These equations, can now be solved following the procedure already described. The introduction of the power law scattering leads us to the algebraic system:

$$\delta_{n'0}+n\mu_0 f^{\mathrm{s}(n-1)}=(2l+1)a_n(n+1)f^{\mathrm{s}(n)} \tag{17}$$

$$n[lf_{l-1}{}^{\mathrm{I}(n-1)}+(l+1)f_{l+1}{}^{\mathrm{I}(n-1)}]$$
$$=(2l+1)a_l(N+1)f_l{}^{(n)}-(2l+1)\delta_{l;0,\ldots,N}[a_n(N+1)-a_n(l)]f_l{}^{\mathrm{I}(n)}$$
$$-\left(\frac{2l+1}{2}\right)\delta_{l;0,\ldots,N}\mathrm{P}_l(\mu_0)[a_n(N+1)-a_n(l)]f_l{}^{\mathrm{s}(n)} \tag{18}$$

where

$$\delta_{l;0,\ldots,N}\equiv\sum_{l=0}^{N}\delta_{l,t}$$
$$f_l{}^n=F_l{}^n[E(E^{2m}/NC_m)^{n+1}]^{-1}$$
$$a_n(l)=\int_0^{\gamma}\mathrm{d}x[1-(1-x)^{1+2m(n+1)}\,\mathrm{P}_l(g)]x^{-1-m}. \tag{19}$$

Notice that for a given order N in the SKA we have a finite number of terms in the Legendre expansion for any spatial moments and that an infinite number of terms will be needed if the SKA is not used. A further advantage of the SKA is the removal of the straight-ahead component of the flux, so F^{I} is a smoother function of the angle than F, which was our goal in using this approximation.

To illustrate the convergence of the synthetic kernel, the spatial moments calculated with kernels of different order are shown in the Appendix.

Having solved equations (2) and (3) by the means of these procedures, we are in a position to define the angular distribution of the energy reflection coefficient for back-scattering and sputtering. After redefining $\mu_0\rightarrow-\mu_0$, since μ_0 is negative for the emitted particles, we have

$$R_{\mathrm{EB}}(\mu_0)=F(x=0,-\mu_0,E)\,\mu_0/E \tag{20}$$
$$R_{\mathrm{ES}}(\mu_0)=F'(x=0,-\mu_0,E)\,\mu_0/E$$

which are formally related to those defined in equation (6) as follows:

$$R_{\mathrm{Eb}}=\int_0^1\mathrm{d}\mu_0 R_{\mathrm{EB}}(\mu_0);\qquad R_{\mathrm{Es}}=\int_0^1\mathrm{d}\mu R_{\mathrm{ES}}(\mu_0).$$

We have to point out that when writing the energy reflection coefficient, we intentionally omitted other variables such as the projectile energy and the angle of incidence. When μ_0 appears explicitly, it is to remind the reader that the function is dependent on such a quantity.

An analytical calculation can be made for the back-scattering component if we use the simplest SKA, that is, the synthetic kernel of order zero and the $m=0$ power cross-section. If we apply a Fourier transformation to equation (14) over the spatial variable, that changes to

$$\delta(\mu-\mu_0)E-\mathrm{i}k\mu\bar{F} = N\int \sigma(E,T)\,\mathrm{d}T[\bar{F}(k,\mu,E,\mu_0)-(k,\bar{F}\mu',E-T,\mu_0) \times g-(1-g)\bar{F}_0(k,T,\mu_0)] \tag{21}$$

where

$$\bar{F}(k,\mu,E,\mu_0)=\int_{-\infty}^{+\infty}\exp(-\mathrm{i}kx)F(x,\mu,E,\mu_0).$$

Introducing the scattering law

$$\sigma(E,T)=C_0/T$$

and assuming

$$\bar{F}(k,\mu,E,\mu_0)=\bar{f}(k,\mu,\mu_0)E \tag{22}$$

we find

$$\delta(\mu-\mu_0)-\mathrm{i}k\mu\bar{f}=a\bar{f}-b\bar{f}_0 \tag{23}$$

where

$$a=a_1(1)$$

$$b=a_1(1)-a_1(0)$$

which have been defined by equation (19) and in this case have to be calculated for $m=0$.

We notice at this point that from equation (19) and equation (21):

$$R_{\mathrm{EB}}(\mu_0)=f(x=0,\mu,-\mu_0)\mu_0. \tag{24}$$

After some rearrangement equation (22) may be written as

$$\bar{f}=[\delta(\mu-\mu_0)+f_0a]/(a+\mathrm{i}k\mu) \tag{25}$$

which after integration over all $\mu(-1;1)$, gives

$$\bar{f}_0=(a+\mathrm{i}k\mu_0)^{-1}+2\bar{f}_0k\tan^{-1}(k/a)\,k^{-1}. \tag{26}$$

From this and from equation (23) we arrive at

$$\bar{f}=\frac{\delta(\mu-\mu_0)}{a+\mathrm{i}k\mu_0}+\frac{b}{(a+\mathrm{i}k\mu_0)(a+\mathrm{i}k\mu)[1-(2b/k)\tan^{-1}(k/a)]}.$$

Now, f can be obtained from $\bar{f}$ by applying the inverse Fourier transformation formula, which for $x=0$ is

$$f(x=0,\mu,\mu_0)=(1/2\pi)\int_{-\infty}^{+\infty}\mathrm{d}k\bar{f}(k,\mu,\mu_0). \tag{27}$$

This can be solved by Cauchy's integral theorem or by numerical methods.

3. Results and discussion

3.1. Total yields

Figure 1 depicts the energy reflection coefficient from equation (5) together with other theoretical results and experimental data. It can be seen in a quantitative way that, as

expected (Bottiger *et al* 1971, Hildebrandt and Manns 1976), the lighter the projectile the greater the contribution of back-scattering to the energy reflection. Agreement between theories should not be sought, since approaches are different. However, they all describe the experimental results within the error of the approximation used. At small mass ratios, theories overestimate energy reflection because they neglect electronic energy loss. With respect to Sigmund's calculation it can be easily seen that his R_E, defined as the fraction of the incoming energy deposited in the negative half-space, underestimates the reflected energy with an error of the order of R_E^2. On the other hand our calculation leads to an overestimation with an error of the order of R_E^3. The difference between these two approaches does not appear in figure 1, since problems connected with the 'multiple passage' in the infinite medium become important at much smaller mass

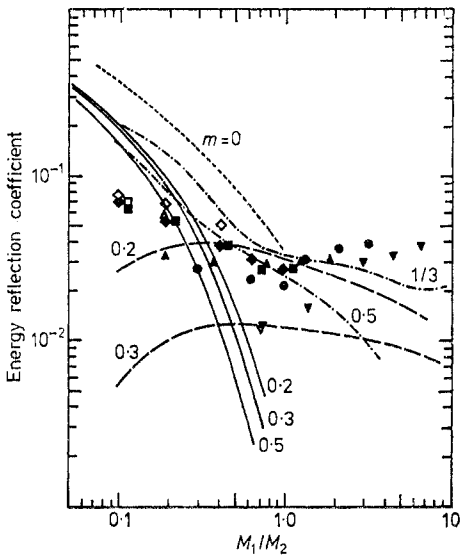

Figure 1. Energy reflection coefficient, total yields. Experimental: full symbols, Andersen (1970) for 30 keV ions; open symbols, Hildebrandt and Manns (1976) for 12 keV He and 9 keV Ne upon different targets. Theory: this work, back-scattering component R_{Eb} (full curves) and sputtering component R_{Es} (dashed curves); other work: Sigmund (1968) chain curves (R_E) and Williams (1979) dotted curve (R_{Eb}). The m exponent of the power scattering law used is on each curve.

ratios. It should be noticed in figure 1, that there is not a well defined border between the regions where back-scattering or sputtering dominate the energy reflection. Nevertheless, we can say that the reflected energy is due to back-scattering at mass ratios smaller than 0·2, and to sputtering at mass ratios greater than 0·6. This conclusion is of course only valid within the elastic collision energy range.

Discrepancies at large mass ratios $M_1/M_2 > 1$ should be attributed to the use of the polynomial approximation with a gaussian basis to reconstruct the energy flux function, since in these cases, large asymmetries must be expected for such a function as a consequence of the almost rectilinear motion of the projectile. Figure 1 also shows Williams' theoretical results (Williams 1979) which overestimate the reflected energy as a result of the use of the simplest SKA which makes the scattering too isotropic, resulting in an increase of the back-scattering probability.

The fact that R_E increases at small M_1/M_2, showing an opposite behaviour to the sputtering yields, as was pointed out in an early publication (Sigmund 1968), becomes understandable now from the consideration of the back-scattering component.

3.2. Angular distribution

We can see in figure 2 measurements by Hildebrandt and Manns on the angular distribution of reflected energy for Cu, Zn and Pb targets under 5 to 14 keV Ne, Ar and Kr ion bombardment at normal incidence. In these experiments, the emission angle was measured from the normal to the surface: we will refer to it by its cosine μ_0. The data were plotted in figure 2 normalised to the value at $\mu_0=1$ and divided by μ_0 in order to emphasise departures from a cosine-like distribution. We note that a possible error in the presentation of the experimental data arises from the fact that the results for $\mu_0=1$ were

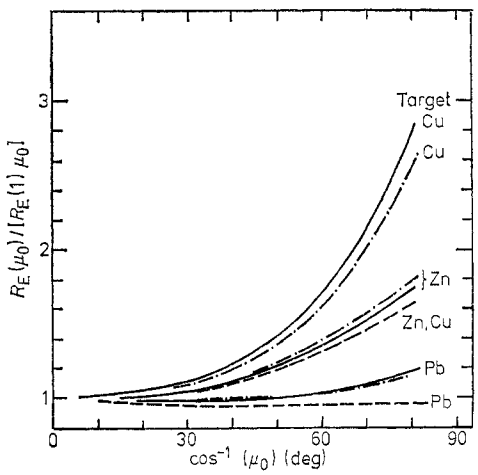

Figure 2. Energy reflection. Angular distributions for Cu, Zn and Pb targets under 5–14 keV Ne, Ar and Kr ion bombardment at normal incidence, from Hildebrandt and Manns (1977). μ_0 is the cosine of the emission angle from the normal to the surface. Data are normalised to the value at $\mu_0=1$ and divided by μ_0 to show up departures from a cosine-like distribution. Projectile: Kr, full curves; Ar, chain curves; Ne, broken curves.

obtained by an extrapolation procedure. Since a cosine distribution is expected when an isotropic flux of energy is just beneath the surface, deviations from such a distribution are a measure of anisotropy. Theoretical calculations are also depicted in figures 3 and 4 for the back-scattering and sputtering contributions, respectively.

Let us analyse now, the experimental data with the aid of our calculation contained in figures 1 and 3 taking the two extreme experimental cases on the mass ratio variable. Firstly, for Ne upon Pb where $M_1/M_2=0{\cdot}097$, the reflected energy is mostly due to back-scattering according to figure 1. In this case we can see in figure 3(*a*) that a small deviation from a cosine-like distribution is expected, and that is what the experiment shows. Secondly, for Kr upon Cu, where $M_1/M_2=1{\cdot}3$, we are, according to figure 1, in the sputtering region. For this case, and taking into account that at the average reduced energy corresponding to such measurements, $\epsilon\sim0{\cdot}03$, the 1/3 power potential should be taken, figure 3(*b*) shows, like the experiment, an overcosine behaviour.

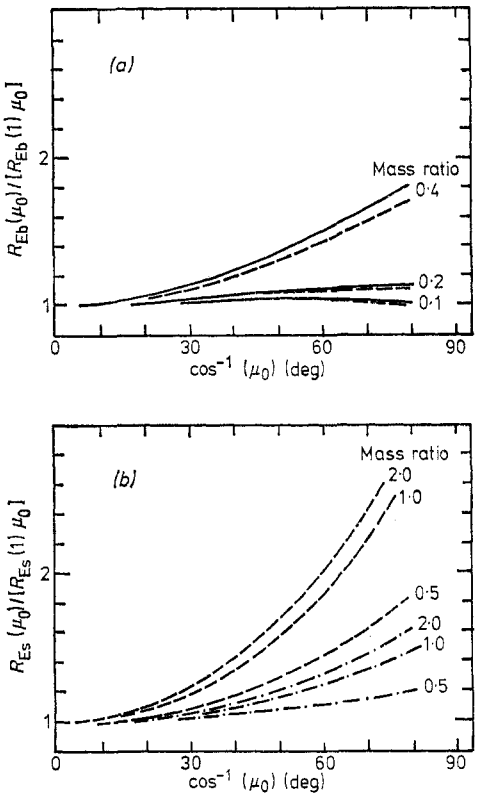

Figure 3. Theoretical evaluation of the angular distribution of (*a*) the back-scattering component R_{Eb} (μ_0) of energy reflection; full curve $m=1/2$, broken curve $m=1/3$; (*b*) the sputtering component R_{Es} (μ_0); broken curve $m=1/3$, chain curve $m=0{\cdot}2$.

In figure 4 we compare our analytical results, i.e. equation (27), with other theoretical works (McCracken *et al* 1969, Williams 1979). Williams (1979) used the Wiener–Hopf technique to solve the forward transport equation in a half-space of stopping material; in this case the reflected energy for normal incidence is given by the formula

$$R_{EB}(\mu_0)=\frac{c}{2}\frac{H(\mu_0)H(1)}{(1+\mu)} \tag{28}$$

where $H(x)$ is Chandrasekhar's function (Chandrasekhar 1960) and c is defined as

$$c=b/a$$

which, obviously, is a function of the mass ratio. It should be pointed out that $H(x)$ also depends on c and so the quantity

$$R_{EB}(\mu)(R_{EB}(1)\,\mu)^{-1}=2H(\mu)/H(1)(1+\mu) \tag{29}$$

still depends on the mass ratio.

McCracken and Freeman (1969) calculated the energy and angular distribution for light ions back-scattering from solids. They used the single collision approximation, a velocity-proportional inelastic energy loss and Rutherford scattering cross-section. From

this work we can easily derive

$$R_{EB}(\mu)(R_{EB}(1)\mu)^{-1} \sim 4(1+\mu)^{-2} \tag{30}$$

which is exact in the limit $M_1/M_2 = 0$.

The main features of our results, i.e. figure 3(*a*) are reproduced by equations (29) and (30), i.e. the larger the mass ratio the greater the anisotropy of the distributions. The advantage of analytical treatments results from the fact that the spatial dependence of the energy flux is solved exactly, furthermore, the Wiener–Hopf technique overcomes the multiple passage problem. However, one must recognise that the simplifying assumption applied to the scattering law makes these analytical procedures only approximate.

A word should be said on some implications of the anisotropy observed for the

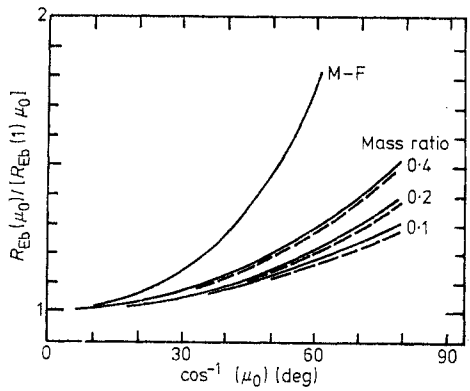

Figure 4. Angular distribution of energy reflected for the back-scattering component R_{Eb} obtained from analytical procedures. Full curves, this work using a Fourier transformation and $m=0$. Dashed curves, Williams (1979) using the Wiener–Hopf technique for a half-space and $m=0$. Curve M–F, results derived from the work of McCracken and Freeman (1969).

energy flux of the sputtering component. The formula

$$N(E, \mu_0) = E\mu_0/(E+U_0)^3 \tag{30}$$

where U_0 is the binding energy, has been used to describe the energy and angular distribution of sputtered atoms (Sigmund 1977), however it will not describe the aforementioned anisotropy. This is important to keep in mind, especially when one is dealing with processes where high energy sputtered atoms play an important role, as in secondary ion and photon emission (Gries and Rüdensauer 1975, Wittmaack 1977, Carter *et al* 1978).

4. Conclusion

The separation of the two components of the reflected energy has been possible by solving the transport equation for the kinetic energy flux. Thus, the energy reflection coefficient was evaluated for both back-scattering and sputtering, and the relative importance of each of them upon the mass ratio variable has been shown. It will be interesting to improve the theoretical treatment for the sputtering component, since the polynomial approximation used appears to have its limitations. In addition we should include

Table 1. Spatial moments of the angular distribution for $M_1/M_2=0{\cdot}1$ and $N=0$–10 synthetic scattering kernel order.

	$\theta_0\approx 0°$					$\theta_0=80°$				
N	$f^{I(0)}$	$f^{I(1)}$	$f^{I(2)}$	$f^{I(3)}$	$f^{I(4)}$	$f^{I(0)}$	$f^{I(1)}$	$f^{I(2)}$	$f^{I(3)}$	$f^{I(4)}$
0	0·318333	0·023254	0·042455	0·013648	0·025905	0·313333	0·065028	0·044742	0·028215	0·029505
1	0·217060	0·022462	0·023024	0·009583	0·010425	0·342586	0·071772	0·040064	0·023496	0·019968
2	0·274769	0·022560	0·025732	0·009090	0·011230	0·308061	0·068612	0·039271	0·022105	0·019094
3	0·234116	0·022535	0·024840	0·009095	0·010938	0·307422	0·068355	0·039264	0·022105	0·018965
4	0·265839	0·022545	0·025263	0·009096	0·010988	0·322204	0·069251	0·039399	0·022146	0·018982
5	0·239603	0·022539	0·025020	0·009095	0·010971	0·318870	0·069125	0·039378	0·022141	0·018981
6	0·262106	0·022541	0·025175	0·009095	0·010978	0·310902	0·068753	0·039336	0·022133	0·018979
7	0·242309	0·022540	0·025068	0·009095	0·010974	0·315292	0·068916	0·039354	0·022135	0·018979
8	0·260049	0·022541	0·025146	0·009095	0·010977	0·319568	0·069082	0·039369	0·022138	0·018980
9	0·243930	0·022540	0·025087	0·009095	0·010975	0·315113	0·068936	0·039356	0·022136	0·018979
10	0·258736	0·022541	0·025133	0·009095	0·010976	0·313223	0·068871	0·039351	0·022135	0·018979
∞	0·251637	0·022541	0·025114	0·009095	0·010976	0·315631	0·068942	0·039356	0·022135	0·018980

Table 2. Spatial moments of the angular distribution for $M_1/M_2=0{\cdot}5$ and $N=0$–10 synthetic scattering kernel order.

	$\theta_0=0°$					$\theta_0=80°$				
N	$f^{I(0)}$	$f^{I(1)}$	$f^{I(2)}$	$f^{I(3)}$	$f^{I(4)}$	$f^{I(0)}$	$f^{I(1)}$	$f^{I(2)}$	$f^{I(3)}$	$f^{I(4)}$
0	0·071343	0·007378	0·011226	0·004566	0·007901	0·071343	0·019683	0·012127	0·009348	0·009294
1	−0·038866	0·001832	−0·004167	0·000533	−0·002089	0·097737	0·028657	0·014771	0·010887	0·009335
2	0·055251	0·003776	0·004988	0·001404	0·002448	0·041424	0·019513	0·011099	0·007913	0·006963
3	−0·018273	0·003169	0·000449	0·001268	0·000608	0·040268	0·018713	0·011054	0·007931	0·006813
4	0·040427	0·003379	0·002850	0·001303	0·001308	0·067621	0·021700	0·011848	0·008329	0·007056
5	−0·008234	0·003290	0·001440	0·001291	0·001021	0·061444	0·021287	0·011724	0·008278	0·007041
6	0·033412	0·003335	0·002346	0·001296	0·001156	0·046699	0·020054	0·011480	0·008195	0·007004
7	−0·003105	0·003309	0·001722	0·001293	0·001085	0·054796	0·020591	0·011584	0·008225	0·007014
8	0·029479	0·003324	0·002174	0·001295	0·001126	0·062549	0·021134	0·011670	0·008248	0·007022
9	−0·000057	0·003312	0·001833	0·001294	0·001100	0·054486	0·020659	0·011597	0·008231	0·007017
10	0·026919	0·003318	0·002098	0·001294	0·001117	0·051043	0·020448	0·011569	0·008224	0·007015
∞	0·014049	0·003319	0·001982	0·001294	0·001109	0·055452	0·020673	0·011590	0·008224	0·007014

electronic energy loss, particularly for the back-scattering component which is the most affected.

Angular distributions of the reflected energy have also been evaluated for the two components, which allows us to explain quite well recent measurements. Further experimental data on the angular distribution of R_E for high energy light ions would be interesting in order to see if anisotropic effects appear as expected theoretically.

Appendix

Convergence of the synthetic scattering kernel

To show the convergence of the synthetic scattering kernel series, we present in tables 1 and 2 the spatial moments of the angular distribution function calculated for $M_1/M_2 = 0{\cdot}1$ and 0·5, respectively, and for the emission angles 0 and 80°. The order of the synthetic kernel covers the range from 0 to 10. The limit for $N = \infty$ is obtained numerically from those first eleven terms by using an extrapolation subroutine.

Comparing tables 1 and 2 we can see that small ratios lead to a better convergence; this is a consequence of a more isotropic collision in the laboratory co-ordinate system.

Acknowledgments

The authors are grateful to the International Atomic Energy Agency for financial support which made possible the visit of M M R Williams to the Centro Atómico Bariloche.

References

Andersen H H 1970 *Radiat. Effects* **3** 51–9
Andersen H H, Lenskjaer T, Sedenius G and Sorensen H 1976 *J. Appl. Phys.* **47** 13–6
Bottiger J, Davies J A, Sigmund P and Winterbon K B 1971 *Radiat. Effects* **11** 69–78
Carter G, Armour D G and Snowdon K J 1978 *Radiat. Effects* **35** 175–87
Chandrasekhar S 1960 *Radiative Transfer* (New York: Dover)
Gries W H and Rüdensauer F G 1975 *Int. J. Mass. Spectrom. Ion Phys.* **18** 111–27
Hildebrandt D and Manns R 1976 *Phys. Stat. Solidi* a K155–7
—— 1977 *Radiat. Effects* **31** 153–6
Littmark U and Maderlechner G 1976 *Proc. Phys. Ionized Gases Symp., Dubrovnik*
McCracken G M and Freeman N J 1969 *J. Phys. B: Atom. Molec. Phys. ser.* 2 **2** 661–8
Robinson J E 1974 *Radiat. Effects* **23** 29–36
Schou J, Sorensen H and Littmark U 1978 *J. Nucl. Mater.* **76–77** 359–64
Sidenius G 1974 *Phys. Lett.* A **49** 407–10
Sigmund P 1968 *Can. J. Phys.* **46** 731–7
—— 1977 *Inelastic Ion-surface Collisions* ed N H Tolk, J C Tully, W Heiland and C W White (New York: Academic Press) pp 121–52
Sorensen H 1976 *J. Appl. Phys.* **47** 13–6
Tanaka S, Murakami Y and Shibata T 1978 *Japan. J. Appl. Phys.* **17** 183–9
Vukanic J and Sigmund P 1976 *Appl. Phys.* **11** 265–72
Williams M M R 1979 *Ann. Nucl. Energy* **6** 145–73
—— 1978 *J. Phys. D: Appl. Phys.* **11** 2455–63
Winterbon K B, Sigmund P and Sanders J B 1970 *K. Danske. Vidensk. Selsk., Mat.-Fys. Meddr.* **37** (14)
Wittmaack K 1976 *Inelastic Ion-surface Collisions* eds N H Tolk, J C Tully, W Heiland and C W White (New York: Academic Press) pp 153–99.